Journal of Electronic Materials (2024) 53:2533–2543
https://doi.org/10.1007/s11664-024-10968-3

ORIGINAL RESEARCH ARTICLE

Research on a High-Threshold-Voltage AlGaN/GaN HEMT with P-GaN Cap and Recessed Gate in Combination with Graded AlGaN Barrier Layer

Zhichao Chen[1] · Lie Cai[1] · Kai Niu[1] · Chaozhi Xu[1] · Haoxiang Lin[1] · Pengpeng Ren[1] · Dong Sun[1] · Haifeng Lin[1]

Received: 13 August 2023 / Accepted: 24 January 2024 / Published online: 5 March 2024
© The Minerals, Metals & Materials Society 2024

Abstract

Due to the enhanced-mode (E-mode) operation, AlGaN/GaN high-electron-mobility transistors (HEMTs) are considered to be safer for circuit operation. In order to improve the threshold voltage (V_{th}) of the device, this work provides a hybrid gate structure HEMT by embedding a P-GaN cap on the etched graded AlGaN barrier layer. Through simulation calculations, the P-GaN cap (thickness of P-GaN = 50 nm, concentration of P-type = 2×10^{18} cm^{-3}) and the aluminum (Al) composition (Al:0.3 → 0.24), in the graded AlGaN barrier layer were optimized. Although simulation calculations show that the optimized P-GaN layer can significantly increase the device's V_{th} to 8.6 V and transconductance (g_m) to 94.7 mS/mm, the device exhibits a lower saturation current (I_{sat}). Therefore, to improve the output characteristics of the devices, the addition of an N-well in the GaN channel layer of such structures was proposed. It can increase the device's source–drain current while maintaining a steady V_{th}. Compared with the HEMT structure/combined P-GaN cap with recessed gate and a graded AlGaN barrier layer, the device with the added N-well exhibits a significant improvement of 11.2% in the saturation current (I_{sat} = 718 mA/mm). The results demonstrate that HEMT structures combining recessed gates and P-GaN with N-well have promising applications in next-generation high-power devices.

Keywords E-mode · AlGaN/GaN HEMT · P-GaN cap · graded AlGaN barrier layer · N-well

Introduction

Gallium nitride (GaN) has emerged as an excellent candidate for high-power and high-temperature applications due to its wide bandgap. It also possesses high breakdown field strength and high electron saturation velocity.[1–3] These properties make GaN-based high-electron-mobility transistors (HEMTs) potential candidates for next-generation power electronic devices in applications such as power supplies, photovoltaic inverters, and motor drives.[4] HEMT devices formed by AlGaN/GaN heterostructures at the two-dimensional electron gas (2DEG) are naturally in the conducting state, which increases power losses and poses challenges to circuit safety.[5] However, enhancement-mode HEMTs[6] have been developed to address these issues. They not only reduce the complexity and cost of circuit design in applications such as radio frequency (RF) and low-noise power amplifiers, but also significantly improve circuit safety and system reliability in high-power switching applications. Moreover, enhancement-mode HEMTs can alleviate the P-channel deficiency in nitride semiconductors. As a result, a growing number of researchers are exploring enhancement-mode HEMTs. Currently, there are several methods to achieve device enhancement mode: recessed gate structures,[7] technology of P-GaN cap,[8] F^{-} implantation technology,[9] and polarization engineering techniques.[10] However, the temperature reliability of devices using fluorine implantation is not suitable for practical applications.[11,12] Polarization engineering techniques have extreme process complexity and cost, making them impractical. The recessed gate technique, while effective, results in a thinner barrier layer due to etching of the AlGaN barrier, causing significant gate leakage current and affecting gate swing and device reliability. On the other hand, P-GaN gate technology employs a P-GaN layer with an activated hole concentration that effectively depletes the

✉ Lie Cai
2011111001@xmut.edu.cn

[1] School of Opto-electronic and Communication Engineering, Fujian Provincial Key Laboratory of Optoelectronic Technology and Devices, Xiamen University of Technology, Xiamen 361024, China

2DEG at the AlGaN/GaN interface, rendering the gate non-conductive under zero bias voltage.[13] Su et al.[14] successfully achieved enhancement-mode HEMT devices by employing heavily doped P-GaN cap layers, resulting in a threshold voltage as high as 4.3 V and a maximum drain–source current of 208 mA/mm. However, the elevated doping concentration of Mg in the P-GaN layer introduces defects,[15–21] leading to a decrease in device performance. Moreover, many related studies have been reported focusing on individual device parameters, and achieving high threshold voltages and drain–source currents simultaneously still poses significant challenges. Therefore, in this paper, we propose a hybrid gate structure combining P-GaN with a recessed gate, and determine the optimal P-GaN cap layer thickness and concentration, leading to a significant improvement in the V_{th} of the HEMT device. In addition, the Al component in the graded AlGaN barrier layer is optimized to reduce the remote scattering effect[22] and improve the electron mobility in the channel. Finally, an N-well is added to the GaN channel layer, effectively increasing the source–drain current of the device. The structure with a P-GaN gate grown on an etched AlGaN barrier layer and an N-well inserted in the GaN channel was realized using Silvaco TCAD (technology computer-aided design) simulation software. This not only significantly increases the V_{th} and g_m of the device but also enhances the maximum drain–source (saturation) current.

Device Structure

Figure 1a, b, and c illustrate the architecture of structure A, consisting of a conventional MIS-recessed gate HEMT; structure B, the recessed gate HEMT covered with a P-GaN layer ($Al_{0.3}Ga_{0.7}N/GaN$); and structure C, the P-GaN cap and recessed gate HEMT with a graded AlGaN layer ($Al_{0.30\rightarrow0.24}Ga_{0.70\rightarrow0.76}N/GaN$). The mole fraction of Al in the AlGaN barrier layer of structure A is 0.24. The mole fraction of Al in the AlGaN barrier layer of structures B and C is 0.3, and the P-GaN cap layer

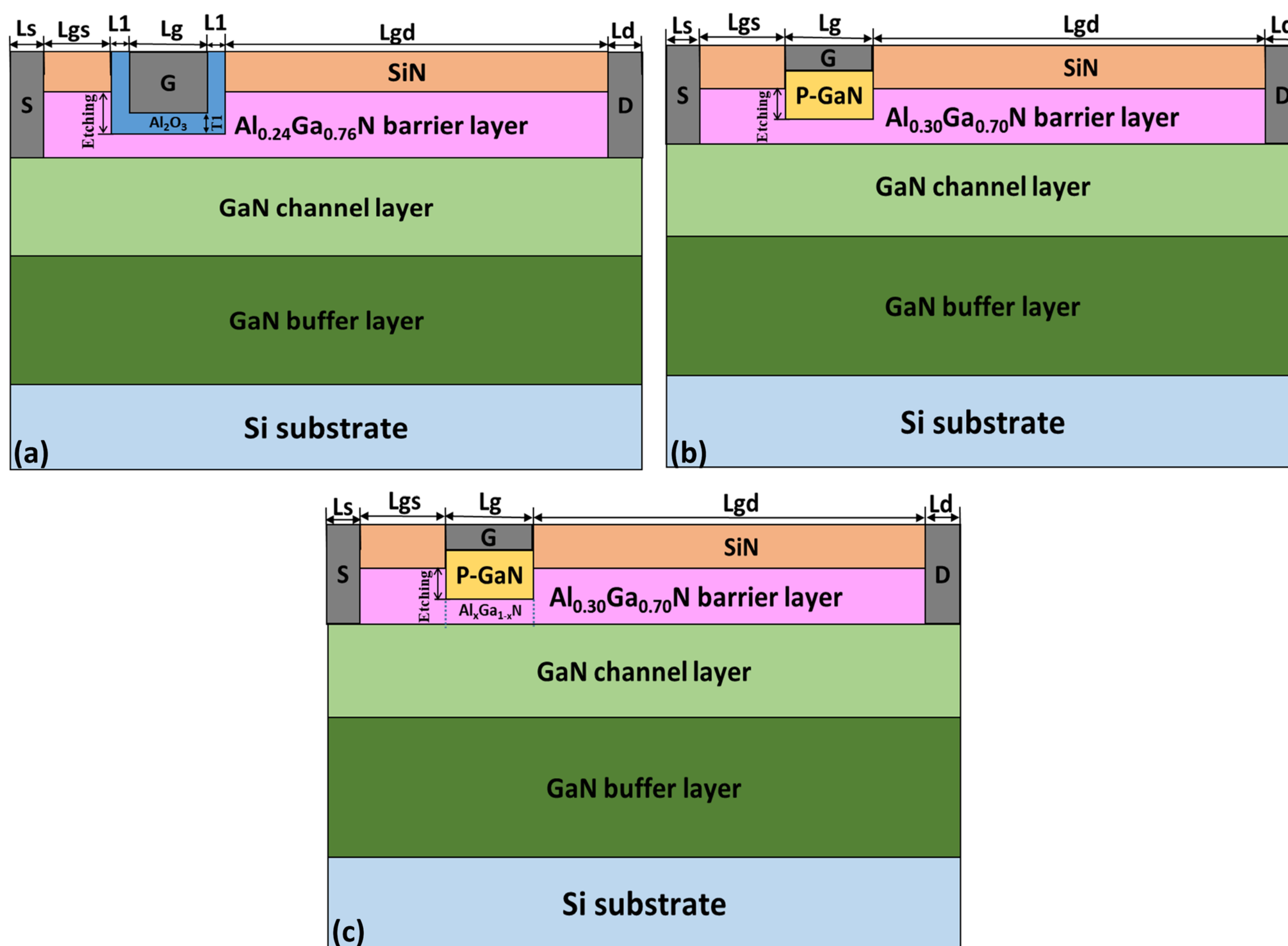

Fig. 1 The structure cross sections of the three devices: (a) structure A: a conventional MIS-recessed gate HEMT, (b) structure B: the recessed gate HEMT covered with a P-GaN layer HEMT ($Al_{0.3}Ga_{0.7}N/GaN$), and (c) structure C: the P-GaN cap and recessed gate HEMT with the graded AlGaN layer HEMT structure ($Al_{0.30\rightarrow0.24}Ga_{0.70\rightarrow0.76}N/GaN$).

is doped with a P-type concentration of 1×10^{18} cm^{-3}. Among them, the GaN buffer layer is unintentionally doped. Table I summarizes the detailed information of the three main structural parameters (a), (b), and (c).

Simulation Model

In this study, we employed the Silvaco ATLAS TCAD tool for 2D simulations.[23] The numerical solution was performed for the Poisson equation, electron continuity equation based on the drift–diffusion (DD) model.[24] The transport equations were solved using the drift–diffusion model,[25] and all calculations in the simulations were based on Fermi–Dirac statistics. Additionally, the Shockley–Read–Hall (SRH) model was utilized to simulate the impact of traps in the bandgap on carrier recombination,[25] and a polarization model was employed to simulate the polarization charges along the heterojunction interface. Considering that the electron mobility in the GaN channel varies with the electric field strength, we considered the effect of the electric field on the electron mobility of the nitride in our simulations and chose a specific field-dependent mobility model. We used the Silvaco ATLAS simulation software to simulate the transfer characteristics of the conventional AlGaN/GaN HEMT and compared the results with previously reported experimental data.[26] As shown in Fig. 2, the results demonstrate excellent agreement between the simulation and experimental data, indicating that the physical parameters chosen in our simulations are consistent with the actual conditions.

Results and Discussion

The polarization model is crucial for the simulation of GaN-based HEMT devices. In Fig. 3, the polarization charge distribution at the AlGaN/GaN heterojunction interface is illustrated for structure B and structure C. The spontaneous polarization arises from the asymmetry along the interface of the wurtzite crystal, while the piezoelectric polarization results from the stress and strain caused by the lattice mismatch between the GaN and AlGaN layers. In the absence of an external electric field, the total polarization intensity

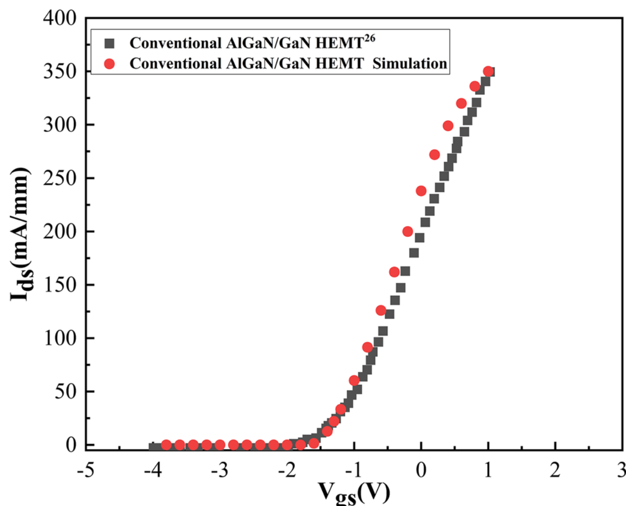

Fig. 2 I_d–V_g characteristic comparison of conventional AlGaN/GaN HEMT[26] with TCAD simulation for validation at V_{ds} = 2 V, V_g = −4 ~ 1 V.

Table I The detailed information on the three main structural parameters (a), (b), and (c)

Parameters	Unit	Value of structure A	Value of structure B	Value of structure C
Source length (Ls)	μm	1	1	1
Distance from gate to source (Lgs)	μm	3	3	3
Gate length (Lg)	μm	1.99	2	2
Thickness of the Al_2O_3 dielectric layer (T1)	nm	1	–	–
Width of the Al_2O_3 dielectric layer (L1)	nm	5	–	–
Distance from gate to drain (Lgd)	μm	9	9	9
Drain length (Ld)	μm	1	1	1
Length of the P-GaN layer (Lp)	μm	–	2	2
Thickness of the P-GaN layer	nm	–	50	50
Al component of the AlGaN barrier layer under the gate	mol	0.24	0.30	0.3 → 0.24
Etching depth of the AlGaN barrier layer	nm	17	10	10
Thickness of AlGaN barrier layer	nm	20	20	20
Thickness of the GaN channel layer	μm	0.4	0.4	0.4
Thickness of the high-resistance GaN buffer layer	μm	2.6	2.6	2.6

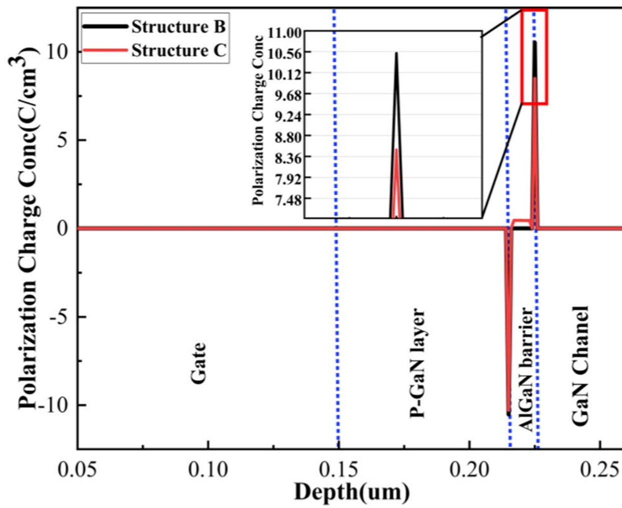

Fig. 3 Polarization-induced charge profile along the vertical axis.

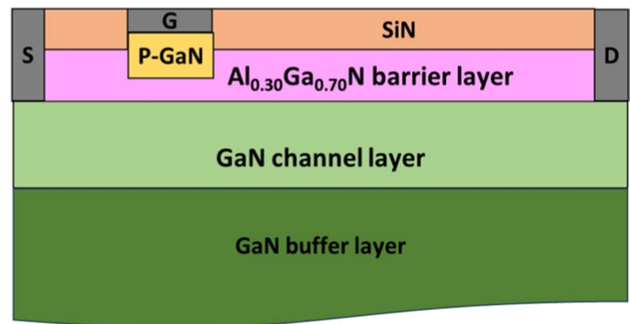

Fig. 4 Schematic of structure B.

(P_{Tol}) is obtained by adding the spontaneous polarization strength (P_{SP}) and the piezoelectric polarization strength (P_{PE}). The 2DEG at the interface of the AlGaN/GaN HEMT heterojunction can be described by the polarization charge formula, Eq. 1:

$$\sigma = P_{\text{spont (AlGaN)}}(x) - P_{\text{spont (GaN)}}(0) + P_{\text{pie (AlGaN)}}(x) \tag{1}$$

Here, the spontaneous polarization strength of the GaN layer is $P_{\text{spont(GaN)}} = -0.034$, and the spontaneous polarization of the AlGaN layer is $P_{\text{spont(AlGaN)}} = -0.052x - 0.034$.

The piezoelectric polarization intensity acting on the AlGaN barrier layer due to the lattice mismatch in the AlGaN/GaN heterojunction can be expressed by Eq. 2:

$$P_{\text{pie}}(\text{AlGaN}) = 2\frac{a_s - a_0}{a_0}\left(E_{31} - \frac{C_{13}}{C_{33}}E_{33}\right) \tag{2}$$

Here, x represents the mole fraction of Al in the AlGaN layer, E_{31} and E_{33} are piezoelectric constants, C_{13} and C_{33} are elastic constants, a_0 and a_s are the lattice constant in the strained layer and the substrate lattice constant, respectively.

$$V_{\text{th}} = \varphi_B - \Delta E_c - \frac{qN_{D_{\text{AlGaN}}}d^2_{\text{AlGaN}}}{2\varepsilon_0\varepsilon_{\text{AlGaN}}} - \frac{\sigma}{\varepsilon_{\text{AlGaN}}}d_{\text{AlGaN}} \tag{3}$$

In Eq. 3, φ_B is the Schottky barrier height of the gate metal, ΔE_c is the conduction band offset at the AlGaN/GaN interface, q is the electron charge, σ is the net polarization charge density at the interface, d is the thickness of the AlGaN barrier, and ε_0 and $\varepsilon_{\text{AlGaN}}$ are the vacuum permittivity and AlGaN permittivity, respectively.

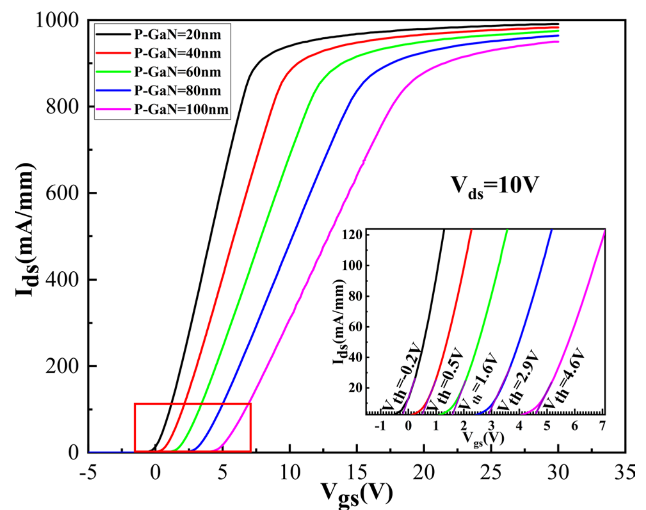

Fig. 5 Transfer characteristic curves of structure B with different thicknesses of P-GaN cap.

DC characteristics of the recessed gate HEMT covered with a P-GaN layer HEMT

We investigated the effect of the thickness of P-GaN on the transfer characteristics of the device when the P-GaN cap was doped with 2×10^{18} cm^{-3} P-type concentration. Figure 4 shows a schematic of structure B.

As shown in Figs. 5 and 6, we consider that when the etching thickness of the AlGaN barrier layer is fixed to 10 nm, the thickness of P-GaN is increased to 20 nm, 40 nm, 60 nm, 80 nm, and 100 nm, respectively. With an increase in the thickness of the P-GaN cap, the distance between the gate and the GaN channel increases, and so does the V_{th}. However, the transconductance decreases significantly. This is because the increased P-GaN thickness weakens the gate control over the channel. Figure 7 presents the relationship between the threshold voltage and transconductance for

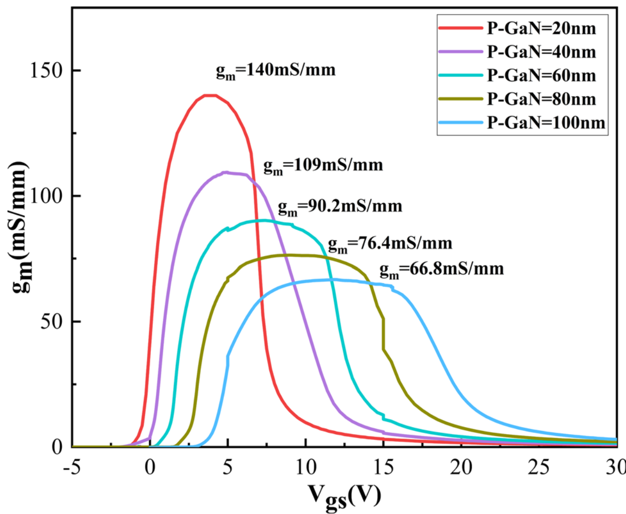

Fig. 6 Transconductance curves of structure B with different P-GaN caps.

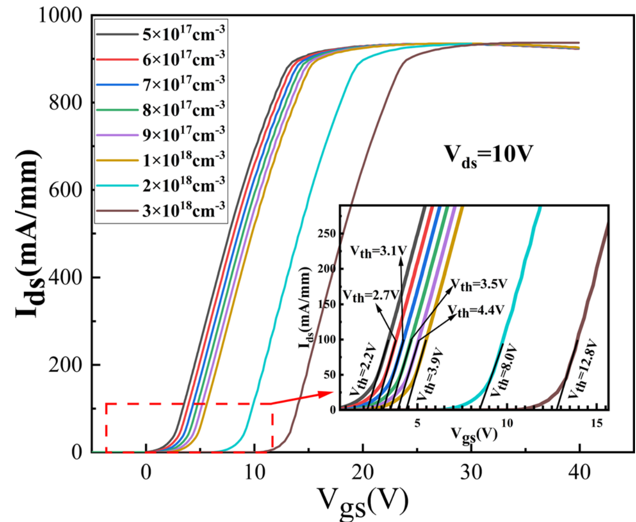

Fig. 8 Transfer characteristics of P-GaN cap with different P-doping concentrations.

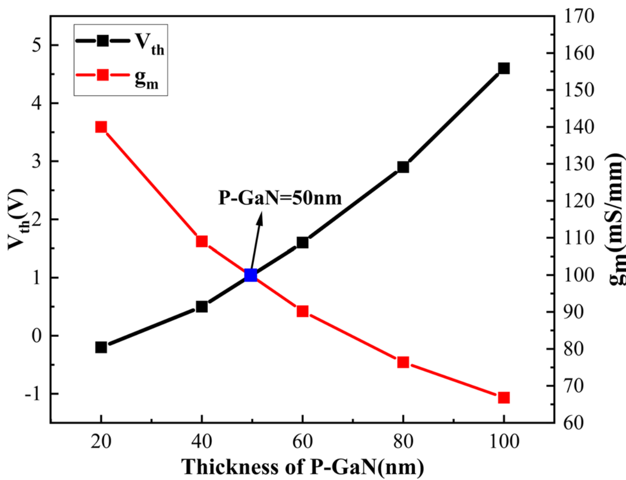

Fig. 7 Relationship between threshold voltage and transconductance for different thicknesses of GaN cap.

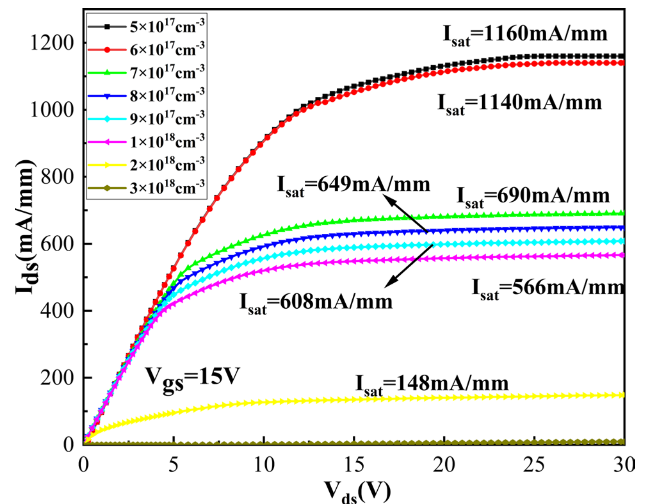

Fig. 9 Output characteristics of P-GaN cap with different P-doping concentrations.

different thicknesses of the GaN cap layer. From Fig. 7, we can conclude that a P-GaN thickness of 50 nm is optimal.

After determining a P-GaN cap thickness of 50 nm, we further discuss the effect of *P*-type concentrations on the device. Figure 8 illustrates the transfer characteristics for different *P*-type concentrations in the P-GaN cap layer. For *P*-type concentrations below 2×10^{18} cm^{-3}, although the threshold voltage increases with the doping concentration, the increase in V_{th} is not significant. However, when the *P*-type concentration is 2×10^{18} cm^{-3} and 3×10^{18} cm^{-3}, the threshold voltage increases significantly to 8 V and 12.8 V, respectively. This is because the hole concentration can deplete the 2DEG under the gate, leading to an increase in the conduction band and the threshold voltage.[27] When the *P*-type concentration is 1×10^{18} cm^{-3}, the 2DEG in the channel is entirely depleted. Thus, at hole concentrations of 2×10^{18} cm^{-3} and 3×10^{18} cm^{-3}, P-GaN increases the energy gap between the conduction band and the Fermi level of the AlGaN/GaN heterojunction. As a result, the gate bias voltage needs to provide additional voltage to reduce the energy gap between the conduction band and the Fermi level, resulting in a significant increase in the threshold voltage. Figure 9 shows the output characteristics for different *P*-type concentrations in the P-GaN cap. Although the device exhibits the highest threshold voltage at a hole concentration of 3×10^{18} cm^{-3}, the source–drain current is practically zero. This is because the high concentration of holes diffuses into

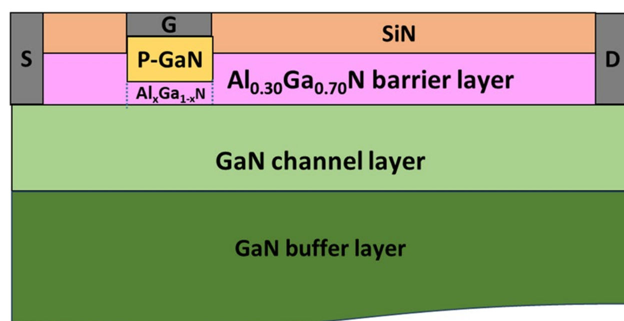

Fig. 10 Schematic of structure C.

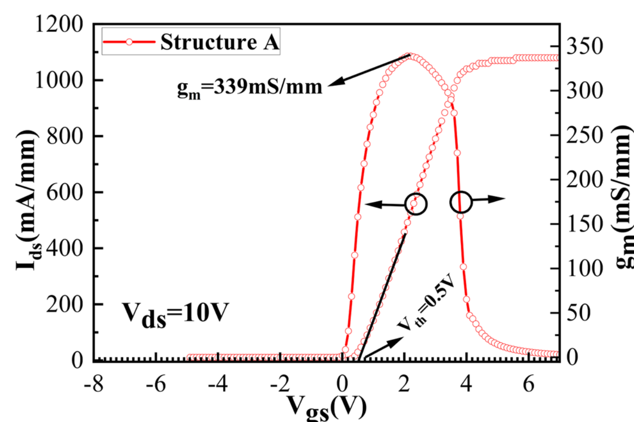

Fig. 11 Transfer characteristics and transconductance curves of structure A.

the GaN channel layer, leading to the recombination of the 2DEG with the holes, resulting in only a few electrons participating in conduction in the channel under the on state, and consequently leading to a very low source-drain current. Additionally, the diffusion of holes into the GaN channel, combined with the lower hole mobility compared with electron mobility, also contributes to the low source–drain current. To strike a balance between the threshold voltage and the source–drain current, we chose a hole concentration of 2×10^{18} cm^{-3} in this study.

To examine the performance of structure C, we propose three different structures: structure A, structure B, and structure C. Figure 10 shows a schematic of structure C. Figures 11 and 12a and b depict the transfer characteristics and transconductance (g_m) curves of the three structures. For structure A, the V_{th} and g_m can reach 0.5 V and 339 mS/mm, respectively. In the case of structure A, when the thickness of the AlGaN barrier layer beneath the gate is etched to 3 nm, the device has a V_{th} of only 0.5 V, indicating the limitation in etching the AlGaN barrier layer to improve the V_{th}. For structure B, the holes in the P-GaN cap can effectively deplete the electrons in the GaN channel layer, significantly increasing the V_{th} to 8.0 V. However, the activation energy of Mg in the P-GaN layer is mostly high (0.15–0.21 eV), and the compensation effect of H in P-GaN prevents the activation concentration of P-GaN from reaching high levels. This is also a critical challenge faced by GaN technology. Therefore, according to Eq. 3, we can reduce the 2DEG beneath the recessed gate caused by polarization charges by reducing the lattice mismatch between the AlGaN barrier layer and the GaN channel layer. The V_{th} of structure C is 8.6 V, which is 0.6 V higher than that of structure B. The transconductance (95.7 mS/mm) of structure C is higher than that of structure B (90.4 mS/mm). This is attributed to the gradual change in the Al composition in the AlGaN barrier layer from 0.3 at the P-GaN/AlGaN interface to 0.24 at the AlGaN/GaN interface. The lower Al composition at the AlGaN/GaN interface reduces the scattering probability for electrons in the GaN channel and thus increases the electron mobility in the GaN channel. Deng et al. reported that increasing the threshold voltage of the device would decrease the density or mobility of 2DEG in the GaN channel, resulting in a decrease in the maximum saturation current output.[28] However, according to Fig. 12a and b, for the transfer and output characteristics of structure C and structure B, not only does the threshold voltage of structure C increase by 0.5 V, but the saturation current of the device is slightly larger than that of structure B. Moreover, structure C also has higher transconductance, which characterizes the controllability of the gate to the channel,[29] and shows that the controllability of structure C to the channel is higher than that of structure B.

To investigate the impact of the gradual change in the Al composition in the AlGaN barrier layer from the P-GaN/AlGaN interface to the AlGaN/GaN interface on the GaN channel, we set up six groups of barrier layers with different Al composition grades: Al: 0.3 → 0.20; 0.3 → 0.22; 0.3 → 0.24; 0.3 → 0.26; 0.3 → 0.28; 0.3 → 0.30. Figure 13a illustrates the transfer characteristics of the six sets of barrier layers with varying Al fractions. The threshold voltage of the device exhibits an increasing trend as the Al tapers from 0.3 to 0.2, attributed to the reduction in the 2DEG concentration resulting from the weakening of the polarization electric field. Figure 13b shows the gate leakage currents of the AlGaN barrier layers with six different Al compositions. The gate leakage current exhibits an increasing trend as the Al content decreases. Notably, the gate leakage current reaches its maximum severity at Al values of 0.20 and 0.22. Conversely, when Al is set to 0.3 and 0.28, the gate leakage current is almost zero. When Al is 0.24 and 0.26, the gate leakage is also considered small for P-GaN gate HEMT devices with V_{gs} greater than 15 V.[30–34] As the AlGaN barrier increases, the gate leakage current is significantly reduced. However, an excessive Al fraction leads to a decrease in the device's threshold voltage. Based on the

Fig. 12 (a) Transfer characteristic, (b) transconductance and (c) output characteristic curves of structure B and structure C.

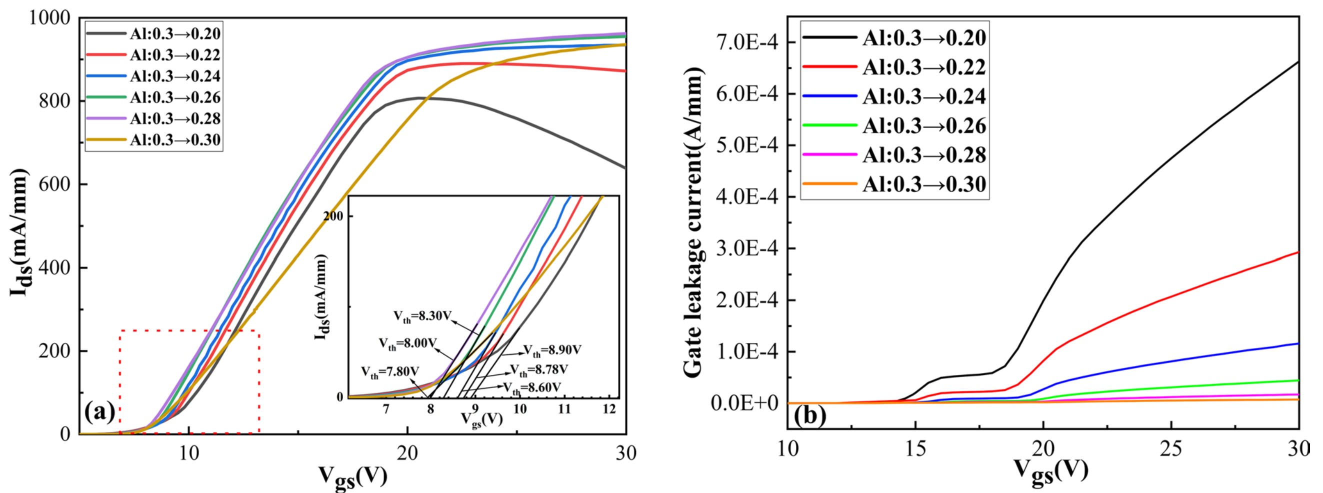

Fig. 13 (a) Transfer characteristic curves of different Al compositions in the graded AlGaN barrier layer, (b) gate leakage current of different Al compositions in the graded AlGaN barrier layer at $V_{ds} = 10$ V and $V_{gs} = 0–30$ V.

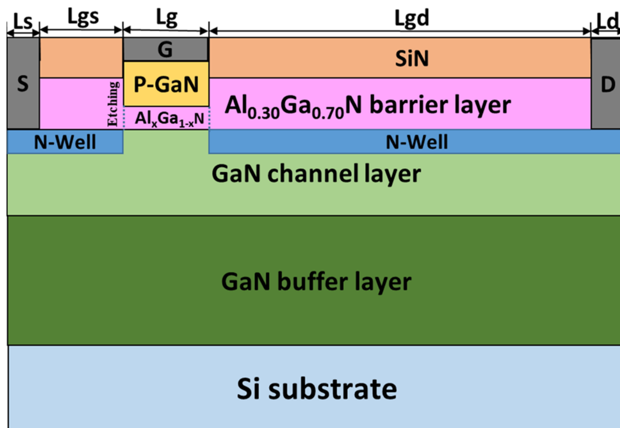

Fig. 14 Structure D: P-GaN cap and recessed gate HEMT with graded AlGaN layer and added N-well in GaN channel.

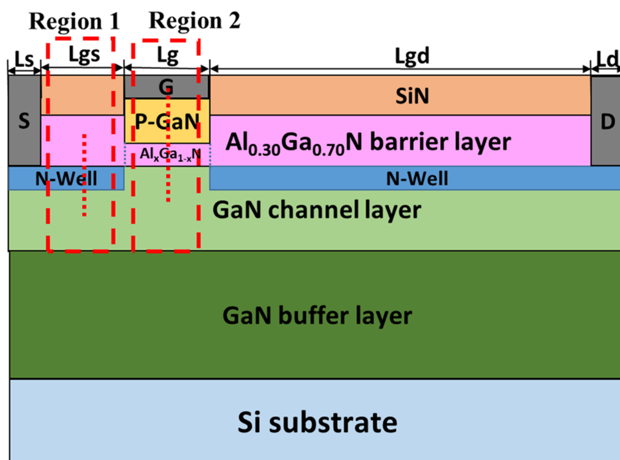

Fig. 15 Schematic of structure D in the simulation software, showing cutline at two locations perpendicular to the *x*-axis.

aforementioned analysis, we determined that an Al composition gradient of 0.24 represents the optimal value for the AlGaN barrier layer.

Figure 14 shows the addition of two 20-nm-thick N-wells with N-doping in the GaN channel of structure D (Fig. 1c). The remaining structural parameters remain unchanged. Figure 15 presents a schematic of structure D with two regions perpendicular to the *x*-axis, designated as region 1 and region 2, in the simulation software. In Fig. 16a and b, the conduction band profiles along the cutline in region 1 and region 2 are shown when N-doping in the N-well is set to 4×10^{18} cm^{-3}. In region 1, the triangular potential well widens below the Fermi level due to the influence of the N-well potential. In region 2, without the presence of an N-well, the rise in the conduction band of the P-GaN cap causes the triangular potential well at the AlGaN/GaN interface to be higher than the Fermi level, leading to the depletion of electrons in the channel. If the N-well is confined within region 1, the doping distribution in the N-well will not affect the electron concentration in the channel below the gate, and thus it will not affect the threshold voltage.

Figure 17 shows the transfer characteristics of I_{ds} (V_{gs}) under different N-doping distributions in the N-well. Although the doping concentration in the N-well does not affect the threshold voltage of the device, the current density of the device increases with the doping concentration in the N-well. Figure 18 illustrates the output characteristics of structure D devices under different *N*-type doping concentrations in the N-well, in which the inset shows the effect of different doping profiles on the N-well drain current at $V_{gs} = 15$ V. The output characteristics of the structure D devices increase with increasing N-doping concentration. This indicates that the addition of the N-well expands the triangular potential well below the Fermi level, thereby increasing the density of carriers participating in the conduction current in the channel. When the N-doping concentration exceeds 8×10^{18} cm^{-3}, the saturation current of the device tends to level off. To achieve a better doping effect, we chose an N-well doping concentration of 8×10^{18} cm^{-3}. Compared with the saturation current of the enhanced structure C device (646 mA/mm) (represented by the light purple dashed line in the inset), the saturation current of the structure D device is significantly higher. When the N-doping concentration is 8×10^{18} cm^{-3}, the saturation current of the structure D device is 718 mA/mm. Although the ionized impurity scattering produced by doping *N*-type impurities in the GaN channel layer affects the carrier mobility in the GaN channel layer, the charge compensation effect of the N-well plays a major role.[35] As a result, the electrons after the ionization of *N*-type impurities participate in the conductivity, which leads to a significant increase in the saturation current of the device. Additionally, Fig. 19 summarizes the threshold voltage and saturation current performance of the proposed composite trench-gate HEMT compared with other reported GaN-based HEMTs.[25,34,36–40] It can be observed that the HEMT of structure D exhibits a significant improvement in output performance at high threshold voltages compared with other GaN-based HEMTs. This points to a wide range of applications of this approach in high-power electronic devices.

Conclusion

In this paper, we propose a HEMT structure combining a P-GaN cap with a recessed gate and an AlGaN barrier layer with a graded Al component. Optimization of the P-GaN cap thickness and P-doping was performed using the Silvaco TCAD simulation tool to achieve an enhanced HEMT device. Additionally, the influence of

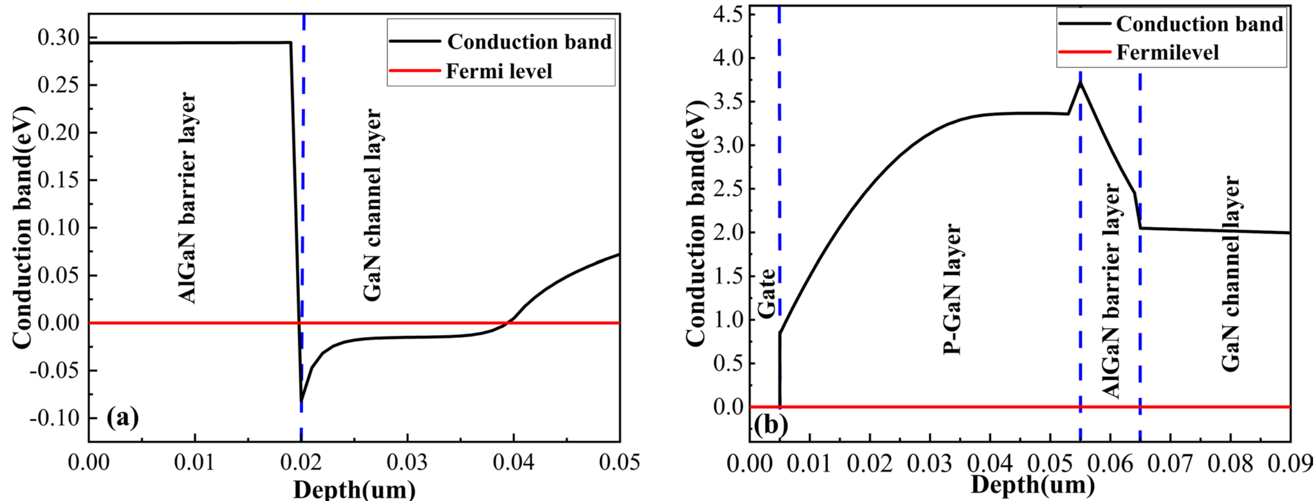

Fig. 16 Conduction band profile of structure D along (**a**) region 1 and (**b**) region 2 below the gate, showing triangular potential wells below the Fermi level at zero gate voltage in Fig. 15.

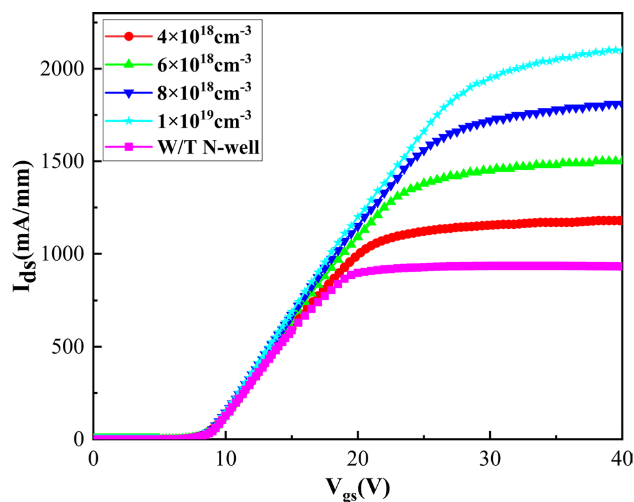

Fig. 17 Transfer characteristic curves for different N-doping concentrations in the N-well.

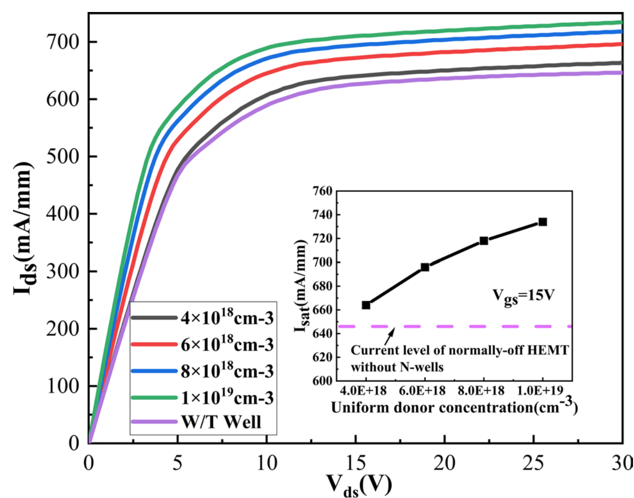

Fig. 18 Output characteristic curves for different N-doping concentrations in the N-well. The inset shows the effect of different doping profiles on the N-well drain current at $V_{gs} = 15$ V.

piezoelectric polarization in the AlGaN barrier layer under the gate electrode was investigated using polarization engineering techniques. Through comparative analysis, it was found that when the Al composition is graded from 0.3 to 0.24, the device exhibits a threshold voltage of $V_{th} = 8.6$ V and a transconductance of $g_m = 97.5$ mS/mm. Most design schemes for enhanced-mode HEMTs significantly impact the source–drain current of the device. Therefore, in the optimized structure mentioned above, an N-well is added to the GaN channel layer, and the effect of the N-doping concentration on the device is discussed. Simulation results demonstrate that the participation of electrons from the N-well in conduction compensates for the channel degradation, thereby improving the device's current density. In particular, the saturation current of the device shows the most significant increase when the N-doping concentration is 8×10^{18} cm^{-3} ($I_{sat} = 718$ mA/mm). Therefore, this structure holds great potential for applications in the field of high-power devices.

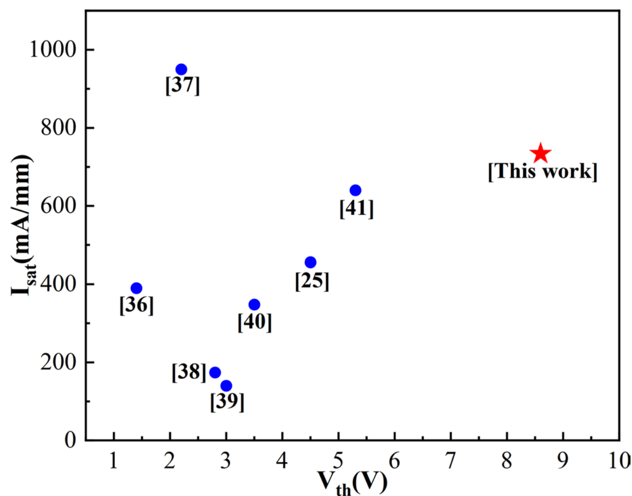

Fig. 19 Comparison of output and transfer characteristics of GaN-based HEMTs. The red star represents this work (HEMT devices of structure D).

Acknowledgments This work was supported by the Natural Science Foundation of Fujian Province (2023J011458, 2021I0025, 2022J011274).

Data Availability The data that support the findings of this study are available from the corresponding authors upon reasonable request.

Conflict of interest The authors declare that they have no conflict of interest.

References

1. O. Ambacher, J. Smart, J.R. Shealy, N.G. Weimann, K. Chu, M. Murphy, W.J. Schaff, L.F. Eastman, R. Dimitrov, L. Wittmer, M. Stutzmann, W. Rieger, and J. Hilsenbeck, Two-dimensional electron gases induced by spontaneous and piezoelectric polarization charges in N- and Ga-face AlGaN/GaN heterostructures. *Appl. Phys.* 85, 3222 (1999).
2. H. Jiang, R. Zhu, Q. Lyu, and K.M. Lau, High-voltage p-GaN HEMTs with OFF-state blocking capability after gate breakdown. *IEEE Electron Device Lett.* 40, 530 (2019).
3. U. Radhakrishna, P. Choi, and D.A. Antoniadis, Facilitation of GaN-based RF- and HV-circuit designs using MVS-GaN HEMT compact model. *IEEE Trans. Electron Devices* 66, 95 (2019).
4. Z. Sunl, Z. Zhang, R. Shenl, Y. Liang, and H. Liang, Performance-improved normally-off AIGaN/GaN high-electron mobility transistors with a designed p-GaN area under the recessed gate. in *IEEE International Conference on Solid-State and Integrated Circuit Technology*. Vol 978, p. 1 (2016).
5. J.P. Ibbetson, P.T. Fini, K.D. Ness, S.P. DenBaars, J.S. Speck, and U.K. Mishra, Polarization effects, surface states, and the source of electrons in AlGaN/GaN heterostructure field effect transistors. *Appl. Phys. Lett.* 77, 250 (2000).
6. F. Le Roux, N. Possémé, P. Burtin, P. Gergaud, and V. Delaye, Characterization of AlGaN/GaN degradations during plasma etching for power devices. *Microelectron. Eng.* 249, 111619 (2021).
7. L. Zhang, Z. Zheng, S. Yang, W. Song, J. He, and K.J. Chen, P-GaN gate HEMT with surface reinforcement for enhanced gate reliability. *IEEE Electron. Device Lett.* 42, 22 (2021).
8. Z. Tang, Q. Jiang, Y. Lu, S. Huang, S. Yang, X. Tang, and K.J. Chen, 600-V normally off SiN_x/AlGaN/GaN MIS-HEMT with large gate swing and low current collapse. *IEEE Electron Device Lett.* 34, 1373 (2013).
9. N. Zeng, Y. Yin, K. Li, F. Liao, and H. Huang, Polarization doping modulated heterojunction electron gas in AlGaN/GaN CAVETs. *Semicond. Sci. Technol.* 35, 095032 (2020).
10. Z. Gao, B. Hou, Y. Liu, and X. Ma, Impact of fluorine plasma treatment on AlGaN/GaN high electronic mobility transistors by simulated and experimental results. *Microelectron. Eng.* 154, 22 (2016).
11. G. Kurt, M.E. Gulseren, T.G.U. Ghobadi, S. Ural, O.A. Kayal, M. Ozturk, B. Butun, M. Kabak, and E. Ozbay, Normally-off AlGaN/GaN MIS-HEMT with low gate leakage current using a hydrofluoric acid pre-treatment. *Solid-State Electron.* 158, 22 (2019).
12. F. Roccaforte, G. Greco, P. Fiorenza, and F. Iucolano, An overview of normally-off GaN-based high electron mobility transistors. *Materials* 12, 1599 (2019).
13. J. Buckeridge, C.R.A. Catlow, D.O. Scanlon, T.W. Keal, P. Sherwood, M. Miskufova, A. Walsh, S.M. Woodley, and A.A. Sokol, Determination of the nitrogen vacancy as a shallow compensating center in GaN doped with divalent metals. *Phys. Rev. Lett.* 114, 016405 (2015).
14. L.-Y. Su, F. Lee, and J.J. Huang, Enhancement-mode GaN-based high-electron mobility transistors on the Si substrate with a p-type GaN cap Layer. *IEEE Trans. Electron. Devices* 61, 460 (2014).
15. B. Sarkar, S. Mita, P. Reddy, A. Klump, F. Kaess, J. Tweedie, I. Bryan, Z. Bryan, R. Kirste, E. Kohn, R. Collazo, and Z. Sitar, High free carrier concentration in p-GaN grown on AlN substrates. *Appl. Phys. Lett.* 111, 032109 (2017).
16. L. Sang, B. Ren, R. Endo, T. Masuda, H. Yasufuku, M. Liao, T. Nabatame, M. Sumiya, and Y. Koide, Boosting the doping efficiency of Mg in p-GaN grown on the free-standing GaN substrates. *Appl. Phys. Lett.* 115, 172103 (2019).
17. N. Tetsuo, I. Nobuyuki, T. Kazuyoshi, K. Keita, and K. Tetsu, Wide range doping control and defect characterization of GaN layers with various Mg concentrations. *J. Appl. Phys.* 124, 165706 (2018).
18. G. Miceli and A. Pasquarello, Self-compensation due to point defects in Mg-doped GaN. *Phys. Rev. B* 93, 165207 (2016).
19. A. Klump, M.P. Hoffmann, F. Kaess, J. Tweedie, P. Reddy, R. Kirste, Z. Sitar, and R. Collazo, Control of passivation and compensation in Mg-doped GaN by defect quasi Fermi level control. *J. Appl. Phys.* 127, 045702 (2020).
20. S. Duguay, A. Echeverri, C. Castro, and O. Latry, Evidence of Mg segregation to threading dislocation in normally-off GaN-HEMT. *IEEE Trans. Nanotechnol.* 18, 995 (2019).
21. J. He, G. Tang, and K.J. Chen, V_{th} instability of p-GaN gate HEMTs under static and dynamic gate stress. *IEEE Electron. Device Lett.* 39, 1576–1579 (2018).
22. Q. Zhou, A. Zhang, R. Zhu, Y. Shi, Z. Wang, L. Liu, B. Chen, Y. Jin, W. Chen, and B. Zhang, Threshold voltage modulation by interface charge engineering for high performance normally-off GaN MOSFETs with high faulty turn-on immunity. in *2016 28th International Symposium Power Semiconductor Devices ICs ISPSD* (IEEE, Prague, Czech Republic, 2016), pp. 87–90.
23. http://www.silvaco.com
24. T. Zine-eddine, H. Zahra, and M. Zitouni, Design and analysis of 10 nm T-gate enhancement-mode MOS-HEMT for high power microwave applications. *J. Sci. Adv. Mater. Devices* 4, 180 (2019).
25. J. Li, Y. Yin, N. Zeng, F. Liao, M. Lian, X. Zhang, K. Zhang, and J. Li, Normally-off AlGaN/AlN/GaN HEMT with a composite recessed gate. *Superlattices Microstruct.* 161, 107064 (2022).
26. Y. Shi, S. Huang, Q. Bao, X. Wang, K. Wei, H. Jiang, J. Li, C. Zhao, S. Li, Y. Zhou, H. Gao, Q. Sun, H. Yang, J. Zhang, W.

Chen, Q. Zhou, B. Zhang, and X. Liu, Normally off GaN-on-Si MIS-HEMTs fabricated with LPCVD-SiN_x passivation and high-temperature gate recess. *IEEE Trans. Electron. Devices* 63, 614 (2016).

27. J.-J. Dai, T.T. Mai, S.-K. Wu, J.-R. Peng, C.-W. Liu, H.-C. Wen, W.-C. Chou, H.-C. Ho, and W.-F. Wang, High hole concentration and diffusion suppression of heavily Mg-doped p-GaN for application in enhanced-mode GaN HEMT. *Nanomaterials* 11, 1766 (2021).
28. S. Deng, J. Wei, C. Zhang, D. Liao, T. Sun, K. Yang, L. Xi, B. Zhang, and X. Luo, High performance flip-structure enhancement-mode HEMT with face-to-face double gates. *Nanoscale Res. Lett.* 17, 73 (2022).
29. F. Wang, W. Chen, R. Sun, Z. Wang, Q. Zhou, and B. Zhang, An analytical model on the gate control capability in p-GaN Gate AlGaN/GaN high-electron-mobility transistors considering buffer acceptor traps. *J. Phys. Appl. Phys.* 54, 095107 (2021).
30. G. Greco, F. Iucolano, and F. Roccaforte, Review of technology for normally-off HEMTs with p-GaN gate. *Mater. Sci. Semicond. Process.* 78, 96 (2018).
31. T.-F. Chang, T.-C. Hsiao, C.-F. Huang, W.-H. Kuo, S.-F. Lin, G.S. Samudra, and Y.C. Liang, Phenomenon of drain current instability on p-GaN gate AlGaN/GaN HEMTs. *IEEE Trans. Electron Devices* 62, 339 (2015).
32. H.-C. Wang, C.-H. Liu, C.-R. Huang, M.-H. Shih, H.-C. Chiu, H.-L. Kao, and X. Liu, Improved I_{on}/I_{off} current ratio and dynamic resistance of a p-GaN high-electron-mobility transistor using an $Al_{0.5}Ga_{0.95}N$ etch-stop layer. *Materials* 15, 3503 (2022).
33. C.-H. Liu, H.-C. Chiu, H.-C. Wang, H.-L. Kao, and C.-R. Huang, Improved gate reliability normally-off p-GaN/AlN/AlGaN/GaN HEMT with AlGaN cap-layer. *IEEE Electron. Device Lett.* 42, 1432 (2021).
34. F. Lee, L.-Y. Su, C.-H. Wang, Y.-R. Wu, and J. Huang, Impact of gate metal on the performance of p-GaN/AlGaN/GaN high electron mobility transistors. *IEEE Electron. Device Lett.* 36, 232 (2015).
35. S. Hamady, F. Morancho, and B. Beydoun, Localized buried p-doped region for E-mode GaN MISHEMTs. *J. Comput. Electron.* 22, 190–198 (2022).
36. K. Sehra, V. Kumari, M. Gupta, M. Mishra, D.S. Rawal, and M. Saxena, A Π-shaped p-GaN HEMT for reliable enhancement mode operation. *Microelectron. Reliab.* 133, 114544 (2022).
37. X.-X. Fei, Y. Wang, X. Luo, F. Cao, and C.-H. Yu, Potential study of the enhanced breakdown voltage GaN MISFET based on partial AlN buried layer. *Superlattices Microstruct.* 114, 314 (2018).
38. Y. Jin, F. Zhou, W. Xu, Z. Wang, T. Zhou, D. Zhou, F. Ren, Y. Xia, L. Wu, Y. Li, T. Zhu, D. Chen, R. Zhang, J. Ye, Y. Zheng, and H. Lu, High- *Vth* E-Mode GaN HEMTs with robust gate-bias-dependent *Vth* stability enabled by Mg-doped p-GaN engineering. *IEEE Trans. Electron. Devices* 70, 5596 (2023).
39. J. Li, Y. Yin, F. Liao, M. Lian, X. Zhang, K. Zhang, Y. Xie, Y. Wu, B. Zou, Z. Zhang, and J. Li, 2.57 GW/cm^2 normally-off composite stepped gate GaN-based HEMT with p-GaN buried layer and field plate. *Mater. Sci. Semicond. Process.* 153, 107152 (2023).
40. A. Mohanbabu, N. Mohankumar, D. Godwin Raj, P. Sarkar, and S.K. Saha, Efficient III-Nitride MIS-HEMT devices with high-κ gate dielectric for high-power switching boost converter circuits. *Superlattices Microstruct.* 103, 270 (2017).

Publisher's Note Springer Nature remains neutral with regard to jurisdictional claims in published maps and institutional affiliations.

Springer Nature or its licensor (e.g. a society or other partner) holds exclusive rights to this article under a publishing agreement with the author(s) or other rightsholder(s); author self-archiving of the accepted manuscript version of this article is solely governed by the terms of such publishing agreement and applicable law.